Expert Systems With Applications 202 (2022) 117052

Contents lists available at ScienceDirect

Expert Systems With Applications

journal homepage: www.elsevier.com/locate/eswa

Range-aided ego-centric collaborative pose estimation for multiple robots ☆

Andreas Papadimitriou [a,*], Sina Sharif Mansouri [b], George Nikolakopoulos [a]

[a] Robotics & AI Team, Department of Computer, Electrical and Space Engineering, Luleå University of Technology, Luleå SE-97187, Sweden
[b] Research and Development Engineer at the Autonomous Driving Lab in Scania Group, Sweden

ARTICLE INFO

Keywords:
Relative pose estimation
UWB
Ego-centric estimation
Sensor fusion

ABSTRACT

Robots' simultaneous relative pose estimation has become an essential step in most robotic-oriented problems, such as map merging, collision avoidance, path planning, and multi-Simultaneous Localization and Mapping (SLAM). This article addresses the problem of 3D and ego-centric relative pose estimation for a team of robots equipped with Ultra WideBand (UWB) nodes. More specifically, the article introduces a novel optimization framework to obtain pose information based on the embodiment of UWB ranges, without relying on any fixed external infrastructure configuration of UWB anchors on the surrounding environment. In the proposed method, we demonstrate the validity through the utilization of a Micro Aerial Vehicle (MAV) and a ground vehicle that are equipped with multiple UWB transceivers, and each platform simultaneously acts as a based anchor for the other platform for extracting an ego-centric position estimation of the UWB nodes. Additionally, for the pose estimation, the obtained information is fused with the onboard Inertial Measurement Unit (IMU) measurements on each of the considered robotic platforms. Finally, the efficacy of the proposed theoretical framework is evaluated in multiple experiments, where the aerial and ground platforms are simultaneously and separately navigating, and the ego-centric collaborative pose-estimation is compared with a VICON ground truth positioning system.

1. Introduction

The ability to estimate the relative pose between multiple robots is essential in many problems in robotics, such as the cooperative localization (Kanellakis, Mansouri, & Nikolakopoulos, 2017), mapping (Funabiki, Morrell, Nash, & Agha-mohammadi, 2020), tracking (Kelsey, Byrne, Cosgrove, Seereeram, & Mehra, 2006), path planning, and collision avoidance (Mansouri, Kanellakis, Fresk, Kominiak, & Nikolakopoulos, 2018). In these cases, the fundamental question that should be addressed is the "Where am I?", and in the sequel, the robots should determine their relative position and orientation (pose). This extrinsic information is necessary for the coordination and cooperation of the robotic team, thus resulting in the registration of the measurements in the same frame of reference. The accuracy of relative pose estimation can directly affect the quality of a sensor fusion, mapping, localization, and overall mission.

In general, robotic applications can demonstrate their capabilities in laboratory environments with the presence of high precision and high sampling rate localization, as an example, with the use of Motion Capture (Mo-Cap) systems, which are capable to provide sub mm accuracy. However, the same performance for the robotic platforms cannot be demonstrated in harsh environments, such as SubTerranean (Sub-T) environments (Mansouri, Kanellakis, Kominiak, & Nikolakopoulos, 2020) as the Mo-Cap require infrastructure to be installed on fixed positions beforehand, and their performance is affected by dust and high humidity. Additionally, these dark and featureless environments challenge the Visual Inertial Odometry (VIO) methods, since the cameras do not yield sufficient information (Özaslan et al., 2017).

The Ultra WideBand (UWB) is a low-power, low-cost, low weight, and high coverage range radio technology that can provide cm accuracy for distance/position information. Same as the Mo-Cap systems, this technology requires a fixed installation of anchors for positioning an attached tag (Fresk, Ödmark, & Nikolakopoulos, 2017; Kanellakis, Fresk, Mansouri, Kominiak, & Nikolakopoulos, 2020) to a robot, which makes it not-suitable for Micro Aerial Vehicle (MAV) deployment in unknown environments.

This article proposes a framework for obtaining pose information based on UWB ranges without considering the fixed installation of the anchors on the environment. In the proposed method, the heterogeneous team of robots consisting of MAV and ground vehicle simultaneously update their relative pose, while navigating asynchronous.

☆ This work has been funded by the European Unions Horizon 2020 Research and Innovation Programme under the Grant Agreement No. 869379 illuMINEation.
* Corresponding author.
E-mail addresses: andpap@ltu.se (A. Papadimitriou), sina.sharif.mansouri@scania.com (S.S. Mansouri), geonik@ltu.se (G. Nikolakopoulos).

https://doi.org/10.1016/j.eswa.2022.117052
Received 17 September 2021; Received in revised form 17 January 2022; Accepted 28 March 2022
Available online 12 April 2022

The platforms are equipped with multiple UWB transceivers, and the optimization problem is proposed to solve the multi anchors and tags positioning for a team of robots. The position information from the UWB nodes is fused with on-board Inertial Measurement Unit (IMU) measurements for obtaining an ego-centric pose information that is relative to the constellation of the participating robots.

1.1. Background & motivation

A recent in-depth survey, presented in Shule, Almansa, na Queralta, Zou, and Westerlund (2020) focuses on the UWB-based localization for robots, while it highlights the lack of localization and navigation techniques of heterogeneous multi-robot systems. Few works consider the use of UWB technology for localization in outdoor environments. In Kanellakis et al. (2020) the authors presented an autonomous MAV inspection framework for wind turbines utilizing UWB and IMU sensor to tackle this challenging maintenance scenario of the featureless environment, where VIO cannot provide accurate localization and the large infrastructure limits the usage of Global Positioning System (GPS) sensors. This type of autonomous inspection requires an infrastructure for installing the UWB anchors for the localization of the MAV. The authors of Güler, Abdelkader, and Shamma (2019) study the concept of infrastructure-free localization, between two MAV and relying on UWB measurements, however there is no contribution towards the concept of relative pose, while one robot act as the base estimating the relative position of the second robot. The platforms do not take advantage of inter-robot communication to improve the position estimates, thus reducing the robustness of the overall positioning framework. Similarly, in Guo, Li, and Xie (2020) the authors address the UWB localization for multi MAVs formation, while the motion is limited in the 2D space. In addition, in Nguyen, Hanif Zaini, Wang, Guo, and Xie (2018), the authors aim to provide a relative localization and tracking between a MAV and a ground vehicle, however, this work considers only translation motions of the base frame, resulting in an offset tracking disregarding the kinematics of a Unmanned Ground Vehicle (UGV) motion, which is limited in 2D space, while changes in orientation are not considered.

The relative pose estimation can be tackled as well with camera-based frameworks. In those cases, for a robot to provide continuous relative pose estimates, it is necessary to maintain at all times a Line of Sight (LoS) with the second agent. The authors of Jeong and Kweon (2013) presented a relative pose estimation method for a UGV and a MAV, where the ground platform was equipped with a top-looking fish-eye camera and an IMU, while the aerial platform was equipped with a down-looking ultrasonic sensor and an IMU. This method was evaluated in a landing scenario, which is possible only if the UGV camera maintains sight with the Unmanned Aerial Vehicle (UAV). Another drawback of the vision-based relative pose estimation is the need for calibrated cameras and pose sensors (Pizarro, Eustice, & Singh, 2003). In Song, Choi, and Kim (2016), the authors proposed a vision-based relative localization framework based on ranges from a 2D LiDAR and RGB-depth (RGB-D) camera information. The proposed algorithm is able to provide robust position information from a fixed agent to a moving target. Finally, the authors of na Queralta, Qingqing, Schiano, and Westerlund (2020) presented a collaborative localization scheme based on UWB and VIO, however, this work relies on a UWB fixed infrastructure, while the main focus is the collaborative sensing of the area for dense scene reconstruction purposes.

Table 1 presents a summary of the most similar state-of-the-art works and their main features. Our proposed method relies on robot communication, an integral part of collaborative robotics. Robots can use a communication link not only to localize each other, as proposed but also to share critical information about an unexplored area or signal danger and other required information of a mission. While most studies utilize the UWB technology for localization purposes, either with permanent installation or infrastructure-free environments, there is no use of the attitude information. Merging localization and orientation will provide the pose of a robot. Map merging, 3D reconstruction, loop closure are a few methods that require orientation information, thus increasing the importance of relative pose estimation in a team of robots.

1.2. Contributions

Based on the aforementioned state of the art, the main contributions of this article are threefold. The first contribution stems from the establishment of the theoretical optimization framework for obtaining the position information between multiple UWB nodes and fused ego-centric orientation based on the IMUs information. In a robot agnostic scenario, the relative pose is defined between multiple agents, while the various robots are allowed to perform both translation and rotation without limiting their locomotion capabilities.

The second contribution stems from omitting the need for fixed UWB infrastructure. In the classical concept of the UWB positioning scheme, there is a need of defining anchors and tags, which are used to differentiate between the inertia frame and the client. Contrary, the proposed novel approach does not require any external infrastructure or defining nodes as anchors or tags. Thus, all nodes are active and the concept of simultaneous anchors and tags of each UWB node for collaborative ego-centric localization is novelty introduced.

Finally, the third contribution stems from evaluating the performance of the proposed theoretical framework in a laboratory environment. The obtained experimental results have a significant novelty and impact the ego-centric relative pose estimation. The following link https://youtu.be/NCcWICwgpqk provides a video summary of the overall experimental evaluations.

1.3. Outline

The rest of this article is structured as follows. In Section 2 the multi-robot synergy navigation concept, the key challenges, and the notation are introduced. In Section 3 the mathematical formulation of UWB position estimation. Furthermore, in Section 4, the multi-sensor fusion of UWB and on-board sensors are presented. The experimental evaluations are presented in Section 5. Finally, concluding remarks, as well as future work are discussed in Section 7.

2. Problem formulation & preliminaries

The deployment of robots in harsh and unreachable areas is getting attention especially in subterranean environments (Agha et al., 2021). The robots should navigate, search, and exploit complex underground environments, such as human-made tunnel systems, urban underground, or natural cave networks. These areas can extend many kilometers in length, have irregular geological structures, unpredictable topologies, constrained passages, multiple levels, and vertical shafts. These challenges limit the deployment of a single platform as MAVs have limited flight time and ground vehicles cannot provide all-terrain navigation capabilities. Additionally, these challenges affect the accuracy of localization, mapping, and path planning frameworks as the large, unknown, and harsh environments result in localization uncertainties, drifts in mapping, etc. Thus, there is a need for relative pose estimation between robots, to convert information to the same coordinate frame for each robot.

Deployment of MAVs and ground vehicles with a high level of autonomy in harsh underground environments poses multiple challenges (Kanellakis, Mansouri, Georgoulas, & Nikolakopoulos, 2018; Mansouri et al., 2020), thus, the need for robust localization, stability, and reliability during operation. In order to improve these aspects, the robotics platforms can be equipped with high-end and expensive sensor suites. However, equipping a MAV with multiple additional sensors will affect the cost of the platforms the flight time (Eleftheroglou et al., 2019) and in extent the length of the mission. Thus,

Table 1
State-of-art relative pose and localization.

Reference	Sensors	Method	Odometry	Evaluation	Pros/Cons
Güler et al. (2019)	Three UWB sensors, Laser range sensor	Monte Carlo localization based on a particle profile for a known velocity profile	Relative localization	Simulations & real-world evaluation	No need for permanent installations, No need for robot communication, No altitude information
Guo et al. (2020)	UWB sensors and build in robot sensors	Relative localization based onboard (UWB) ranging and communication (RCM) network	Infrastructure-free cooperative relative localization	Simulations & real-world evaluation	No need for permanent installations
Nguyen et al. (2018)	UWB sensors, IMU, altimeters, optical flow	Relative pose based on sequential fusion	Position and Orientation	Lab experimental Evaluation	No need for permanent installations, Single robot tracking
Jeong and Kweon (2013)	Fish-eye camera and ultrasonic range finder	Relative pose based on fusion	Position and Orientation	Lab experimental Evaluation	No need for permanent installations, always requires LOS.
Song et al. (2016)	RGB-Depth Camera, 2D LiDAR	RGB-D and Lidar measurements fusion, and adaptive color-based particle filter for visual tracking	Relative localization	Lab experimental Evaluation	Provides only position information, requires LOS.

this article proposes the use of UWB technology for obtaining relative pose information from an ego-centric approach. While the UWB system definitely provides lower accuracy data, it is lightweight and a lot cheaper than most of the 3D lidars and high-end cameras. Towards this direction, this article investigates into the problem of relative pose estimation for aerial and ground vehicles, while each platform acts as UWB anchors for the other one. Thus, this article considers the ranges information from both sides instead of the classical approach of fixed anchors positions for tag position estimation.

In this work scalars are presented as non-bold characters such r, or N, while vectors are bold lower-case letters e.g. $\boldsymbol{v}$, $\boldsymbol{x}$ and matrices bold upper-case letters like $\boldsymbol{A}$, $\boldsymbol{B}$. Finally, coordinate frames are distinguished from scalars by the following font $\mathcal{W}$, $\mathcal{S}$.

Following the illustrated notations in Fig. 1, the coordinate frames are denoted as $\{\cdot\}$ and its axes are labeled as $x_\cdot, y_\cdot$ and $z_\cdot$, adopting the frame's label as their subscript.

The UWB coordinate frame is noted as $\mathcal{U}$ and it is coincident with robot/agent 1 coordinate frame $\mathcal{R}_a$. The same robot has attached n_a anchors/transceivers and for $i = 1, \dots, n_a$ the anchors are located at $\boldsymbol{p}_{a,i} = [x_{a,i}, y_{a,i}, z_{a,i}]$ relative to the $\mathcal{R}_a$.

Furthermore n_n nodes are placed on the robot/agent 2 and for $m = 1, \dots, n_n$ the nodes are located at $\boldsymbol{p}_{n,m} = [x_{n,m}, y_{n,m}, z_{n,m}]$ relative to the $\mathcal{R}_a$. The nodes assumed are placed at an offset from the Center Of Gravity (COG) and origin of the coordinate frame $\mathcal{R}_b$ of $\boldsymbol{p}_{o,m} = [x_{o,m}, y_{o,m}, z_{o,m}]$.

The proposed method requires communication among the robots. An additional initialization stage is required if there is a loss of communication for a short duration while the robots are moving. During that initialization stage, the current pose of the estimated robot is required for the re-initialization of the framework. Although there is no need for robots to maintain a direct LoS to each other, walls or large obstacles can partially block or reflect the communication messages among the nodes, and result in degraded estimates (Fresk et al., 2017). Without losing generality, the following assumptions are made: (a) The initial relative pose of the estimated object is known, (b) ranging information among the UWB nodes is available, (c) the positions of the transceivers are kept constant relative to each other on a robot. The UWB frame is created and aligned with the IMU frame.

3. UWB relative position estimation

The UWB technology is used to estimate the distance between two transceivers when they exchange multiple time-stamped messages with each other. We refer to that distance as range $r \in \mathbb{R}^+$ and it is estimated based on the time it takes for a message to travel from one transceiver to another (Mueller, Hamer, & D'Andrea, 2015) one. To localize an object via UWB technology in a 3D-space, at least four UWB anchors are required. As it has been described in Fresk et al. (2017), while three anchors are enough for the localization of an object the fourth anchor is necessary to ensure the uniqueness of the solution.

In this work we consider a team of robots with unique identities (IDs) and present the concept of relative position between two agents a and b. The UWB coordinate frame $\mathcal{U}$ is located on one agent with coordinate frame $\mathcal{R}_a$, while a second agent with $\mathcal{R}_b$ is deployed with multiple UWB nodes and it is the one localized relative to the $\mathcal{R}_a$. As is will be shown in the sequel, the same principals can be followed to provide relative position of $\mathcal{R}_a$ **w**ith **r**espect **t**o (w.r.t) $\mathcal{R}_b$.

3.1. Position of the anchors

Let the agent a with the moving frame $\mathcal{U}$ carrying a set of UWB transceivers. The defined $\mathcal{U}$ is aligned with the IMU of this particular robot and in extent with the robot's origin $\mathcal{R}_a$ i.e. $\boldsymbol{q}_{\mathcal{R}_a\mathcal{U}} = [\boldsymbol{0}_u, 1]^\top$. We will refer to the transceivers of that robot as anchors from now on for clarity purposes. The anchors are placed at an offset from the $\mathcal{R}_a$ denoted as $\boldsymbol{p}^{\mathcal{R}_a}_{a,i}$. While the placement of the anchors is constant, the robot 1 can move and rotate in 3D, thus the updated positions of the anchors w.r.t $\mathcal{W}$ can be calculated from (1).

$$\boldsymbol{p}^{\mathcal{W}}_{a,i} = \boldsymbol{R}(\boldsymbol{q}_{\mathcal{W}\mathcal{R}_a})\boldsymbol{p}^{\mathcal{R}_a}_{a,i} + \boldsymbol{T}(\mathcal{W}\mathcal{R}_a), \tag{1}$$

where $\boldsymbol{R}(\boldsymbol{q}_{\mathcal{W}\mathcal{R}_a})$ denotes the rotation matrix from $\mathcal{R}_a \to \mathcal{W}$ and $\boldsymbol{T}(\mathcal{W}\mathcal{R}_a)$ the translation between the origins of the frames. We can rewrite (1) in a more compact form as:

$$\boldsymbol{p}^{\mathcal{W}}_{a,i} = \boldsymbol{C}\begin{pmatrix} \boldsymbol{q} \\ \boldsymbol{T} \end{pmatrix}(\mathcal{W}\mathcal{R}_a))[\boldsymbol{p}^{\mathcal{R}_a}_{a,i}, 1]^\top, \tag{2}$$

where $\boldsymbol{C}(\cdot)$ would the homogeneous transformation matrix in (3)

$$\boldsymbol{C}\begin{pmatrix} \boldsymbol{q} \\ \boldsymbol{T} \end{pmatrix}(\mathcal{W}\mathcal{R}_a)) = \begin{bmatrix} \boldsymbol{R}(\boldsymbol{q}_{\mathcal{W}\mathcal{R}_a}) & \boldsymbol{T}(\mathcal{W}\mathcal{R}_a) \\ \boldsymbol{0}_{1\times 3} & 1 \end{bmatrix}. \tag{3}$$

The formulation in (2) captures the updates in 3D space of the first robot and uses them to keep updated the state of the moving UWB frame that will be used to obtain the relative position of the second robot as it will be described in the sequel.

3.2. Position of the nodes

In contrast to previous works (Fresk et al., 2017; Guo et al., 2020; na Queralta et al., 2020) which place a single node on the subject robot for estimating its position, in our novel proposed formulation we are using a set of nodes placed at $\boldsymbol{p}^{\mathcal{R}_b}_{n,m}$. With the end goal to estimate the relative position of $\mathcal{R}_b$ w.r.t $\mathcal{R}_a$, which would be $\boldsymbol{p}^{\mathcal{R}_a}_{\mathcal{R}_b}$ we need to express

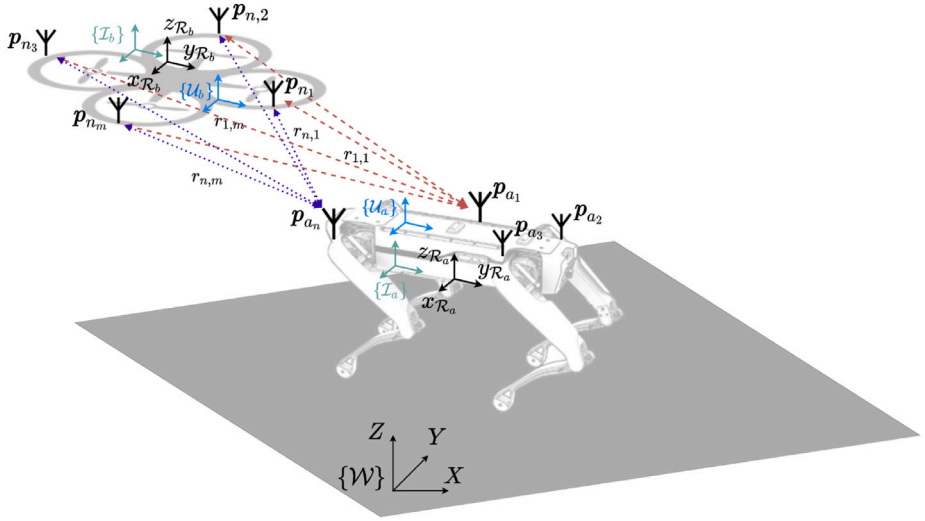

Fig. 1. Relative pose estimation concept based on ranges for multiple robots. Each platform is equipped with multiple UWB transceivers with indication of their ranges among them. Four basic coordinates frames are depicted $\mathcal{R}_{a,b}$ with origin at robots' center of mass, IMU frames $\mathcal{I}_{a,b}$, the origin of the UWB network $\mathcal{U}_{a,b}$ and global frame $\mathcal{W}$.

that position in terms of the *nodes*' position. Let m nodes with positions $\boldsymbol{p}^{\mathcal{U}}_{n,m}$ located at a distance $r_{i,m}$ from an anchor $\boldsymbol{p}^{\mathcal{R}_a}_{a,i}$. To successfully localize the robot b by utilizing all nodes, we could solve m times the following optimization (4).

$$\min(\|\boldsymbol{p}^{\mathcal{R}_a}_{a,i} - \boldsymbol{p}^{\mathcal{U}}_{n,m}\|_2 - r_{i,m})^2, \tag{4}$$

where $\boldsymbol{p}^{\mathcal{U}}_{n,m}$ would be the decision variable. This implies that we have m set of decision variables and of course $\boldsymbol{p}^{\mathcal{U}}_{n,1} \neq \cdots \neq \boldsymbol{p}^{\mathcal{U}}_{n,m}$. Taking into account that UWB provides only position estimates, we would need to translate the position of the nodes to the origin of $\mathcal{R}_b$ to obtain the $\boldsymbol{p}^{\mathcal{R}_a}_{\mathcal{R}_b}$. But the distance measurements between anchors and nodes is far from ideal and it is affected by noise and anomalies, thus the $\boldsymbol{p}^{\mathcal{R}_a}_{\mathcal{R}_b}(m)$ estimate from each node would not result to the same position.

Another approach would be to consider a combined optimization with equality constraints.

$$\begin{aligned}
&\boldsymbol{p}^{\mathcal{U}}_{n,1} - \boldsymbol{p}^{\mathcal{R}_b}_{n,1} = \boldsymbol{p}^{\mathcal{U}}_{n,2} - \boldsymbol{p}^{\mathcal{R}_b}_{n,2} \\
&\boldsymbol{p}^{\mathcal{U}}_{n,2} - \boldsymbol{p}^{\mathcal{R}_b}_{n,2} = \boldsymbol{p}^{\mathcal{U}}_{n,3} - \boldsymbol{p}^{\mathcal{R}_b}_{n,3} \\
&\cdots \\
&\boldsymbol{p}^{\mathcal{U}}_{n,m-1} - \boldsymbol{p}^{\mathcal{R}_b}_{n,m-1} = \boldsymbol{p}^{\mathcal{U}}_{n,m} - \boldsymbol{p}^{\mathcal{R}_b}_{n,m}
\end{aligned} \tag{5}$$

where $\boldsymbol{p}^{\mathcal{R}_b}_{n,m}$ would be the translation constant offset of each node to the origin of $\mathcal{R}_b$. The overall scheme would result to multiple decision variables and a set of constraints.

Lastly our choice was to express the cost function with only the decision variable $\boldsymbol{p}^{\mathcal{R}_a}_{\mathcal{R}_b}$. This could be solved if we transform the origin of the $\mathcal{R}_b$ to the frame of each *node* and express it as function of $\boldsymbol{p}^{\mathcal{R}_a}_{\mathcal{R}_b}$. One can express immediately the relation between $\boldsymbol{p}^{\mathcal{R}_a}_{\mathcal{R}_b}$ and $\boldsymbol{p}^{\mathcal{R}_b}_{n,m}$ into the cost function itself and that would be:

$$J = \left(\|\boldsymbol{p}^{\mathcal{R}_a}_{a,i} - (\boldsymbol{p}^{\mathcal{R}_a}_{\mathcal{R}_b} + \boldsymbol{R}(\boldsymbol{q}_{\mathcal{R}_a\mathcal{R}_b})\boldsymbol{p}^{\mathcal{R}_b}_{n,m})\|_2 - r_{i,m}\right)^2. \tag{6}$$

Following the formulation in (6) there are only three decision variables x_d, y_d, z_d, which are the coordinates of the $\mathcal{R}_b$ w.r.t $\mathcal{R}_a$. Furthermore, since the optimization solves for the same decision three variables, regardless of the node, there is no need for the constraints in (5).

Thus, for a set $\boldsymbol{P}_j$ containing all data of a_n anchors positions, n_n nodes positions, the ranges $r_{i,m}$ among them, and the relative orientation between two robots can be defined as,

$$\boldsymbol{P}_j = \left\{\boldsymbol{p}^{\mathcal{R}_a}_{a,i}, \boldsymbol{R}(\boldsymbol{q}_{\mathcal{R}_a\mathcal{R}_b})\boldsymbol{p}^{\mathcal{R}_b}_{n,m}, r_{i,m}\right\} \tag{7}$$

and the combined optimization for a window of N measurement sets is given in (8).

$$\min_{\{\boldsymbol{p}^{\mathcal{R}_a}_{\mathcal{R}_b}(k)\}} \underbrace{\|\boldsymbol{p}^{\mathcal{R}_a}_{\mathcal{R}_b}(k) - \boldsymbol{p}^{\mathcal{R}_a}_{\mathcal{R}_b}(k-1)\|^2_{\boldsymbol{Q}_0}}_{\text{initial guess}} + \sum_{j=0}^{N-1} J|_{\boldsymbol{P}_j}, \tag{8}$$

where the cost function is enhanced with an *initial guess* term to smooth the solution of $\boldsymbol{p}^{\mathcal{R}_a}_{\mathcal{R}_b}(k)$, which is the decision variable at the time instant k, while with $k-1$ is denoted the previous position of the agent.

3.3. Solving the opposite problem

As stated in Section 1 one can use the acquired ranges among UWB transceivers to solve the reverse problem and gain relative position information for the platform that acts as the UWB anchors $\mathcal{U}$ frame.

The definition can stand vice-versa assuming a second UWB frame $\mathcal{U}_2$ whose origin will be on the second platform coincident to $\mathcal{R}_b$ and the IMU. The same UWB transceivers assigned as nodes before this time are assigned as anchors. The anchors are placed at an offset from the $\mathcal{R}_b$ and denoted as $\boldsymbol{p}^{\mathcal{R}_b}_{a,i}$. Similar to the previous analysis, the robot b is able to move so that the position of the anchors is updated on-line. The rotation and translation can be described by the homogeneous transformation matrix,

$$\boldsymbol{C}\begin{pmatrix}\boldsymbol{q}\\ \boldsymbol{T}\end{pmatrix}(\mathcal{W}\mathcal{R}_b)) = \begin{bmatrix}\boldsymbol{R}(\boldsymbol{q}_{\mathcal{W}\mathcal{R}_b}) & \boldsymbol{T}(\mathcal{W}\mathcal{R}_b)\\ \boldsymbol{0}_{1\times 3} & 1\end{bmatrix}. \tag{9}$$

Furthermore, the set $\boldsymbol{P}_j$ containing all data anchors, nodes, relative rotation between the two agents is the reverse case that is defined as,

$$\boldsymbol{P}_j = \left\{\boldsymbol{p}^{\mathcal{R}_b}_{a,i}, \boldsymbol{R}(\boldsymbol{q}_{\mathcal{R}_b\mathcal{R}_b})\boldsymbol{p}^{\mathcal{R}_a}_{n,m}, r_{i,m}\right\} \tag{10}$$

Similarly, the optimization for a window of N measurement sets is given in (11).

$$\min_{\{\boldsymbol{p}^{\mathcal{R}_b}_{\mathcal{R}_a}(k)\}} \underbrace{\|\boldsymbol{p}^{\mathcal{R}_b}_{\mathcal{R}_a}(k) - \boldsymbol{p}^{\mathcal{R}_b}_{\mathcal{R}_a}(k-1)\|^2_{\boldsymbol{Q}_0}}_{\text{initial guess}} + \sum_{j=0}^{N-1} J|_{\boldsymbol{P}_j}, \tag{11}$$

where the solution of the optimization $\boldsymbol{p}^{\mathcal{R}_b}_{\mathcal{R}_a}(k)$ is the relative position of $\mathcal{R}_a$ w.r.t $\mathcal{R}_b$.

4. Range-aided relative pose estimation

Using the information of the orientation $\boldsymbol{q}_{\mathcal{R}_a\mathcal{R}_b}$, which describes a rotation from the $\mathcal{R}_a$ frame to the $\mathcal{R}_b$ frame, the relative pose is composed as:

$$\boldsymbol{\xi}_{\mathcal{R}_a}^{\mathcal{R}_b} = [\boldsymbol{p}_{\mathcal{R}_b}^{\mathcal{R}_a}, \boldsymbol{q}_{\mathcal{R}_a\mathcal{R}_b}]^\top. \tag{12}$$

The information of each robot sensor suite is fed to the Extended Kalman Filter (EKF)-based sensor fusion module with the goal of improving the accuracy and increasing the robustness against uncertainties and outliers. As an initialization stage the sensors are rotated and translated to the world frame.

4.1. IMU kinematics

While every robotic setup might have different sensor suite, depending on the robot type or/and application scenario, the vast majority of robotic platforms include an IMU sensor. Thus, it can be convenient to estimate inertial odometry providing corrections from additional sensor sources whenever they are available. Similar to Solà (2017), the state vector of the IMU is defined as:

$$\hat{\boldsymbol{x}}_{\text{imu}} = [\boldsymbol{p}_{\mathcal{R}}^{\mathcal{I}^\top}, \boldsymbol{v}_{\mathcal{R}}^{\mathcal{I}^\top}, \boldsymbol{q}_{\mathcal{R}}^{\mathcal{I}^\top}, \boldsymbol{b}_{\omega}^{\mathcal{I}^\top}, \boldsymbol{b}_{a}^{\mathcal{I}^\top}], \tag{13}$$

where the $\boldsymbol{p}_{\mathcal{R}}^{\mathcal{I}}$ and $\boldsymbol{v}_{\mathcal{R}}^{\mathcal{I}}$ are the position and velocities w.r.t to a robot frame $\mathcal{R}$. The rotation of the IMU relative to the robot in quaternion is $\boldsymbol{q}_{\mathcal{R}}$. Furthermore, $\boldsymbol{b}_{\omega}^{\mathcal{I}^\top}$ and $\boldsymbol{b}_{a}^{\mathcal{I}^\top}$ are the biases of gyro and accelerometer respectively.

The kinematics of an IMU-driven platform, adapted from Solà (2017), are provided by the following equations in (14). The measured IMU acceleration $\boldsymbol{a}_m$ and angular rate $\boldsymbol{\omega}_m$ are usually corrupted by noise $\boldsymbol{a}_n$ and $\boldsymbol{\omega}_n$ and the biases described above.

$$\dot{\boldsymbol{p}}_{\mathcal{R}}^{\mathcal{I}} = \boldsymbol{v}_{\mathcal{R}}^{\mathcal{I}} \tag{14a}$$

$$\dot{\boldsymbol{v}}_{\mathcal{R}}^{\mathcal{I}} = \boldsymbol{R}(\boldsymbol{q}_{\mathcal{R}\mathcal{I}})\left(\boldsymbol{a}_m - \boldsymbol{b}_a^{\mathcal{I}} - \boldsymbol{a}_n\right) + \boldsymbol{R}_{\mathcal{W}\mathcal{R}}^\top \boldsymbol{g}_{\mathcal{W}} \tag{14b}$$

$$\dot{\boldsymbol{q}}_{\mathcal{R}\mathcal{I}}^{\mathcal{I}} = \frac{1}{2}\boldsymbol{q}_{\mathcal{R}\mathcal{I}}^{\mathcal{I}} \otimes \left(\boldsymbol{\omega}_m - \boldsymbol{b}_{\omega}^{\mathcal{I}} - \boldsymbol{\omega}_n\right) \tag{14c}$$

$$\dot{\boldsymbol{b}}_a^{\mathcal{I}} = \boldsymbol{a}_w \tag{14d}$$

$$\dot{\boldsymbol{b}}_{\omega}^{\mathcal{I}} = \boldsymbol{\omega}_w \tag{14e}$$

The described system can be written as a function $\dot{\boldsymbol{x}}_{\text{imu}} = f(\boldsymbol{x}, \boldsymbol{u}, \boldsymbol{w})$ with input $\boldsymbol{u} = [\boldsymbol{a}_m - \boldsymbol{a}_n, \boldsymbol{\omega}_m - \boldsymbol{\omega}_n]^\top$ and acceleration and gyro biases with Gaussian white noise $\boldsymbol{w} = [\boldsymbol{a}_w, \boldsymbol{\omega}_w]^\top$.

Considering, the nominal state of the system, where the system is free of noise and perturbations (Solà, 2017) and by linearizing using the small angle approximation of the error quaternion, the error-state kinematics are described in Eq. (15).

$$\delta\dot{\boldsymbol{p}}_{\mathcal{R}}^{\mathcal{I}} = \boldsymbol{v}_{\mathcal{R}}^{\mathcal{I}} \tag{15a}$$

$$\delta\dot{\boldsymbol{v}}_{\mathcal{R}}^{\mathcal{I}} = -\boldsymbol{R}\left[\boldsymbol{a}_m - \boldsymbol{b}_a^{\mathcal{I}}\right]_\times \delta\boldsymbol{\theta} - \boldsymbol{R}\delta\boldsymbol{b}_a^{\mathcal{I}} + \delta\boldsymbol{g} - \boldsymbol{R}\boldsymbol{a}_n \tag{15b}$$

$$\delta\dot{\boldsymbol{\theta}}_{\mathcal{R}\mathcal{I}}^{\mathcal{I}} = -\left[\boldsymbol{\omega}_m - \boldsymbol{b}_{\omega}^{\mathcal{I}}\right]_\times \delta\boldsymbol{\theta} - \delta\boldsymbol{b}_{\omega}^{\mathcal{I}} - \boldsymbol{\omega}_n \tag{15c}$$

$$\delta\dot{\boldsymbol{b}}_a^{\mathcal{I}} = \boldsymbol{a}_w \tag{15d}$$

$$\delta\dot{\boldsymbol{b}}_{\omega}^{\mathcal{I}} = \boldsymbol{\omega}_w \tag{15e}$$

where $[(\cdot)]_\times(\cdot) = (\cdot)\times(\cdot)$ is the skew-symmetric cross product matrix. The state-error $\delta(\cdot)$ defines the difference of the estimated value and the quantity, for example $\delta\boldsymbol{p} = \hat{\boldsymbol{p}} - \boldsymbol{p}$. This procedure defers for the attitude portion, where the difference of quaternions is defined as error-quaternion $\delta\boldsymbol{q} = \boldsymbol{q} \otimes \hat{\boldsymbol{q}}^{-1}$, which can be also written $[1 \quad \frac{1}{2}\delta\boldsymbol{\theta}]$, where $\boldsymbol{\theta} \in \mathbb{R}^3$ is angle vector.

$$\delta\hat{\boldsymbol{x}}_{\text{imu}} = [\delta\boldsymbol{p}_{\mathcal{R}}^{\mathcal{I}^\top}, \delta\boldsymbol{v}_{\mathcal{R}}^{\mathcal{I}^\top}, \delta\boldsymbol{q}_{\mathcal{R}}^{\mathcal{I}^\top}, \delta\boldsymbol{b}_{\omega}^{\mathcal{I}^\top}, \delta\boldsymbol{b}_{a}^{\mathcal{I}^\top}], \tag{16}$$

4.2. UWB positioning fusion

The UWB sensor system provides ranges between the transceivers and through a process described in Section 3 estimates of position are derived. The position information from the UWB is used in combination with the error-state equations. The translational offset between the IMU and the origin of the UWB sub-network is fixed, as the position of the sensor within the platform are always the same. The state for the UWB is:

$$\hat{\boldsymbol{x}}_{\text{uwb}}^{\mathcal{U}} = [\delta\boldsymbol{p}_{\mathcal{R}_i}^{\mathcal{U}}]^\top \tag{17}$$

To compensate for the IMU drifts, commonly appeared in inertial driven systems, we utilize the UWB absolute position measurements. Although, UWB provides drift-free measurements the ranges are affected by noise. The prediction portion of the EKF is based on the IMU measurements. Thus, the system uses the linear and angular accelerations as input $\boldsymbol{u} = [\boldsymbol{a}, \boldsymbol{\omega}]^\top$.

During the prediction stage the future states are estimated based on IMU input $\boldsymbol{u}$ and the states given in (13) as $\dot{\boldsymbol{x}} = f(\boldsymbol{x}, \boldsymbol{u})$ and the predicted covariance is computed by $\boldsymbol{P}_{k+1} = \boldsymbol{F}\boldsymbol{P}_k\boldsymbol{F}^\top + \boldsymbol{Q}$. Where $\boldsymbol{F}$ is the system's jacobian and $\boldsymbol{Q}$ is the covariance zero mean Gaussian process noise.

During the update stage the new state estimates are updated by $\hat{\boldsymbol{x}} = \boldsymbol{x} + \boldsymbol{K}\boldsymbol{y}$ where $\boldsymbol{y}$ is the UWB absolute position and $\boldsymbol{K}$ is the Kalman gain. Thus, during the innovation the UWB states are used for the correction of the predicted states. The full prediction and update equations of a Kalman filter can be found in Yaakov, X., and Thiagalingam (2004), or Reif, Gunther, Yaz, and Unbehauen (1999).

A critical component for using data from different sources is to ensure the correct timing of the data regardless of its arrival, i.e. to compensate for delayed measurements that will affect the prediction stage. Therefore, the timestamps of the onboard computation unit are used for indicating the moment of arrival of each individual measurement for all the sensors. The collected data then is properly injected into a measurement window, which is updated every time a new measurement arrives. A schematic of the measurement update procedure is depicted in Fig. 2.

5. Experimental evaluation

For the evaluation of the theoretical framework presented in Sections 2–4, a sequence of experimental trials was performed in laboratory conditions to prove the performance of the proposed method. The main focus of this evaluation is the pose estimation using the UWB technology with multiple transceivers attached to the robot's main body. Initially, a detailed presentation of the components and configuration used for the experimental sequence will be given. Following the hardware and software specifics, the results of the evaluation will be presented.

5.1. Experimental setup

This article evaluates the localization and relative pose estimation between two robotic platforms with the aforementioned novel methodology. A ground platform, which is a quadruped robot (*Spot*) (Bouman et al., 2020), equipped with a sensor suite able to provide 12-state estimates $\hat{x}_{\text{spot}}$ of pose (position and orientation) and twist (linear and angular velocity) while a set of five UWB nodes is fixed around its body as depicted in Fig. 3. These anchors are placed strategically on the main body to ensure their visibility from all sides of the ground platform. Furthermore, to avoid anchors' individual rotation and translation, when the joints of ground platform are actuated, the anchors are not placed on the legs of the ground platform. Table 2 shows the position of the anchors w.r.t the center of gravity of the ground platform. Each UWB transceiver orientation during installation on the robot does not play a significant role in the overall framework, but the coordinates

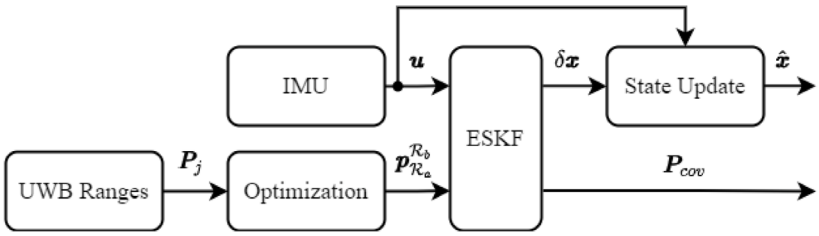

Fig. 2. State update block diagram based on the EKSF fusion of IMU and UWB.

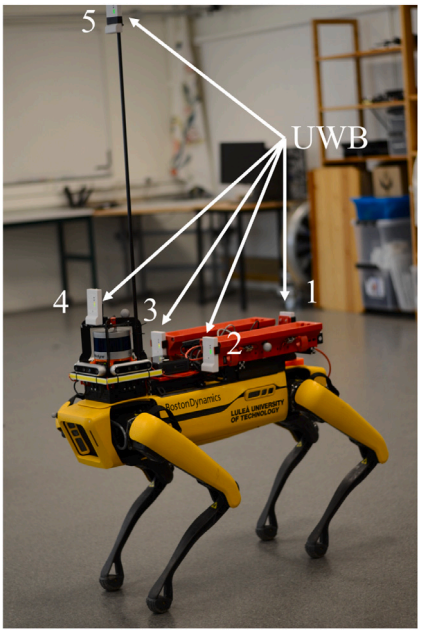

Fig. 3. Quadruped robotic platform equipped with UWB nodes.

Table 2
Position of the installed UWB transceivers on the ground platform w.r.t $\mathcal{R}_a$.

UWB nodes	1	2	3	4	5
x [m]	−0.40	0.30	0.00	0.00	0.21
y [m]	0.00	0.00	−0.12	0.12	0.06
z [m]	0.00	0.19	0.00	0.00	0.95

Table 3
Position of the installed UWB transceivers on the quadcopter w.r.t $\mathcal{R}_b$.

UWB nodes	1	2	3	4
x [m]	−0.05	−0.16	−0.14	0.14
y [m]	0.0	0.21	−0.24	−0.24
z [m]	0.26	0.03	0.03	0.03

of the individual modules govern the selection of the coordinate system. Based on our codes and several Robot Operating System (ROS) packages, we have selected the NWU convention. Subsequently, we selected the position of the individual nodes such that the resulting UWB coordinate frame will be coincident with the IMU frame.

The aerial quadcopter platform is a MAV that is equipped with four UWB nodes, as depicted in Fig. 4. Under each arm of the aerial platform, an UWB node is installed for reasons that are described in Section 3. The nodes have absolute physical distance from the COG of the platform as depicted in Table 3. Similar to the ground platform method for selecting the position for the transceivers, the UWB modules coordinates are such to align the UWB frame with IMU frame following the NWU convention again.

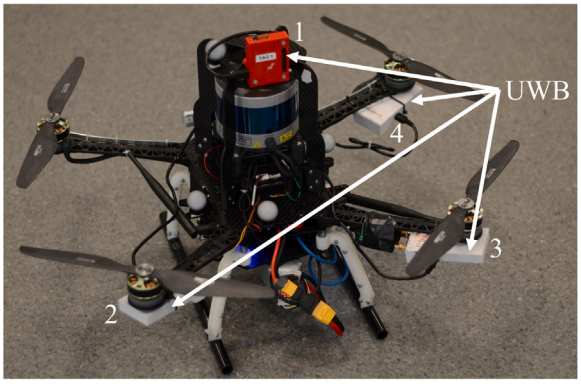

Fig. 4. Quadcopter equipped with UWB nodes.

Initially the quadcopter is docked on the landing station located on top of the ground vehicle, as shown in Fig. 5, while the ground platform is already moving the quadcopter to initialize its position and manually takes-off from the landing station. Three sets of experiments are presented in the sequel. Initially, the quadcopter navigates around, while the ground platform is immobilized, in the second case the quadcopter is immobilized and the ground platform navigates, and in third case both robotic platforms navigate around simultaneous. For the evaluation of the proposed methodology, the Vicon Mo-Cap system is utilized to provide the ground truth of both robots states. The testing facilities consist of 19 Vicon cameras providing measurements with sub-millimeter accuracy at a rate of 100 Hz. Additionally, for comparison with a second commonly used reference system (VIO), we utilize the RealSense Tracking Camera T265, advertised to provide 6 ms latency between movement and reflection of the movement in the pose and 1% error and drifting (Alapetite, Wang, Hansen, Zajaczkowski, & Patalan, 2020).

For the optimization (8), the available tuning parameters are the measurements window, the weight of the *initial guess* and the weight of the current measurement stage. These parameters were selected after iterative tests, and they were kept constant throughout the experimentation process. Considering the rate of the input data, through the ROS framework from UWB devices, which is approximately at 20 Hz, the measurement window N is set at 6. A larger measurement window increases the computation time and on the other hand, selecting a narrow measurement window decreases the overall estimation performance. The contribution of the initial guess is adjusted at $\boldsymbol{Q}_0 = 0.5$ for x, y, z. Increasing further the $\boldsymbol{Q}_0$ is resulting in slight delays on the position changes while setting the weight to zero is resulting in more estimation spikes. The weight of the current localization stage was kept at $\boldsymbol{Q}_w = 1$, as it appeared to give the best estimates on static and slow changes of position estimation tests.

Table 4, shows the three different testing scenarios and the method used to estimate the pose of the platforms. Furthermore, the exact experimental sequence will be described in the sequel before presenting its results.

Table 4
Experimental Scenarios Summary.

	Case 1		Case 2		Case 3	
	Ground platform	Quadcopter	Ground platform	Quadcopter	Ground platform	Quadcopter
Vicon	✓	✓	✓	✓	✓	✓
VIO		✓		✓		✓
UWB	✓	✓	✓	✓	✓	✓
UWB-IMU	✓	✓	✓	✓	✓	✓
Motion		✓	✓		✓	✓

Fig. 5. Quadcopter is located on the landing station on top of the ground vehicle.

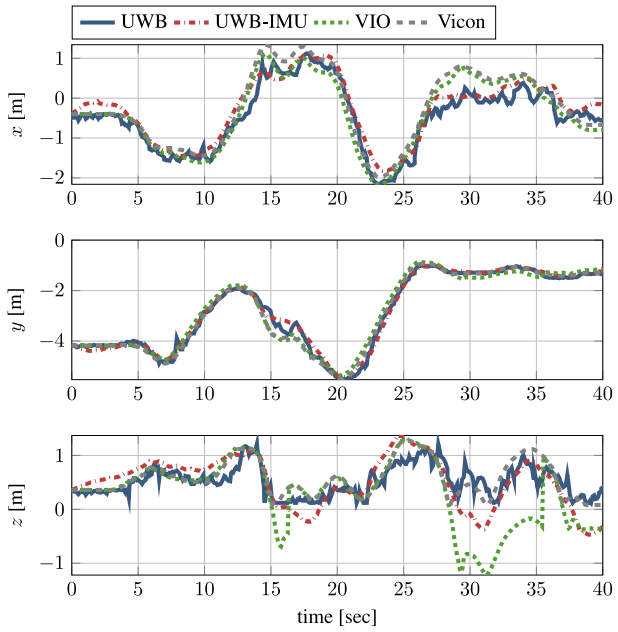

Fig. 6. Case 1 — Estimated global position of the quadcopter with the proposed method with and without fused IMU data versus VIO and Vicon measurements.

5.2. Results

The results of the experimental trials are divided based on three different scenarios. For each case, the description of the scenario is followed by illustrations and a discussion of the results.

5.2.1. Case 1: Quadcopter navigates around the stationary ground platform

For the first case, the ground platform is immobilized, and the quadcopter manually takes off from the landing station and navigates. The pilot performs maneuvers while changing the position and orientation of the quad-copter simultaneously. Fig. 6 depicts the position estimates of the quad-copter in the global frame of the UWB measurements, UWB fused with IMU measurements, referred from now on as UWB-IMU, VIO, and Vicon measurements. Can be noted that UWB and UWB-IMU data follow similar trends to the Vicon measurements. Furthermore, it can be noticed that UWB-IMU appears to be smoother when compared to UWB in all three axes. For comparison purposes, the signal acquired with VIO is illustrated, and it can be noticed that while in x and y-axes, the accuracy is higher compared to z-axis, as in the z-axis, the sudden changes of altitude pushes the height measurements far from the actual value.

Furthermore, Fig. 7 depicts the position estimates error of the quadcopter in the global frame for the same sensors in comparison to the "true" value. The VIO appears to have the lowest error with the exception when the altitude changes aggressively and loses the tracking. The UWB and UWB-IMU have similar performance while UWB-IMU results to less spikes.

For the same case, the rotation error of the quadcopter, relative to the ground platform, is depicted in Fig. 8 as obtained from the fusion of the UWB and IMU measurements. While the error stays under 0.05 [rad] in all cases, there are short peaks. The orientation Root Mean Square Error (RMSE) values are similar for VIO, IMU, UWB-IMU with combined RMSE of 0.032, 0.048, and 0.023 rad, respectively. These error levels are in an acceptable range considering the small differences in the placement of the sensors.

The estimation error of the ground platform pose from UWB and IMU measurements on the aerial platform, as described in Section 3, is presented in Fig. 9. For the first case, the ground platform is not moving. Thus it is expected that ground platforms' position will remain constant. From the error plot, it is observed that the UWB measurements show multiple jumps, which on the other hand, are kept to a minimum with the fused with IMU data. It is worth noting that during the initial seconds, the fused data has higher error until the signal converges after a few position corrections from the UWB arrive. However, the overall error is lower for the UWB-IMU.

The Fig. 10 depicts the relative position error of the quadcopter, when compared to the ground platform, either relying on UWB or UWB-IMU estimates. Overall, the fused with IMU data appear to be smoother from UWB in terms of variations. In addition, it can be noticed that for this experimental trial, the x-axis appears to have a larger drift, while the y-axis of the UWB-IMU has a smaller error compared to the UWB.

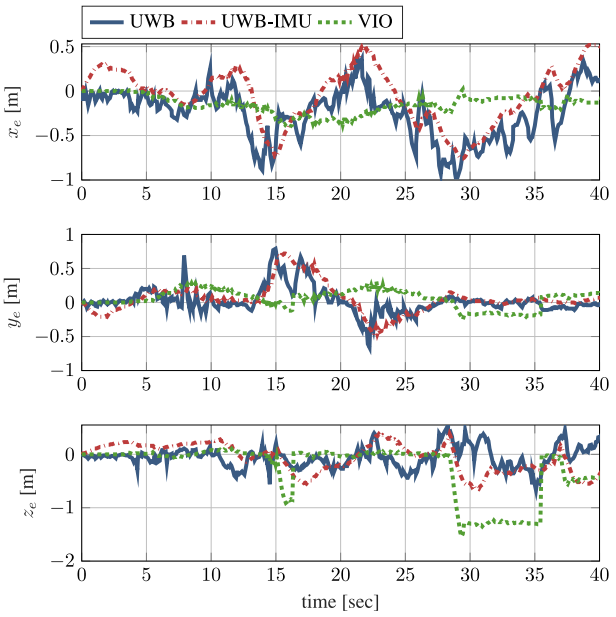

Fig. 7. Case 1 — Estimated global position error of the quadcopter with the proposed method with and without fused IMU data versus VIO.

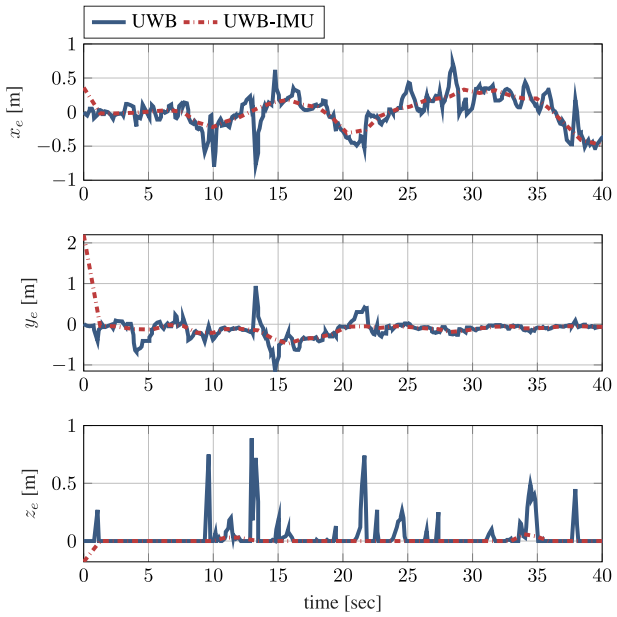

Fig. 9. Case 1 — Estimated global position error of the immobilized ground platform of the proposed method with and without fused IMU.

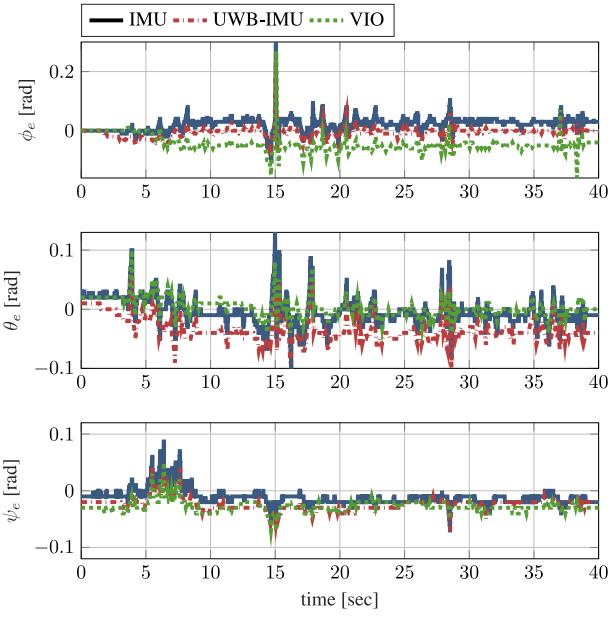

Fig. 8. Case 1 — Rotation error of the quadcopter w.r.t the ground platform.

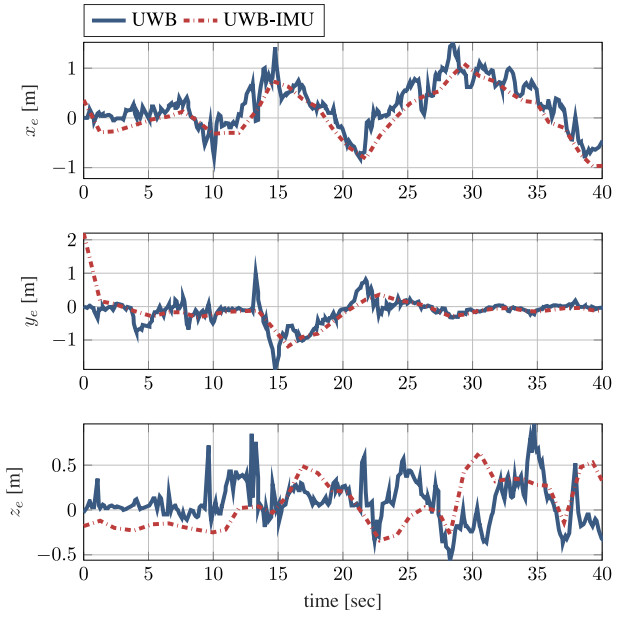

Fig. 10. Case 1 — Estimated relative position error of the quadcopter w.r.t the ground platform of the proposed method with and without fused IMU data.

Table 5 presents the RMSE values between the Vicon measurements and the VIO, UWB, UWB-IMU for both platform. In the first column, it is observed that the localization obtained from UWB and UWB-IMU measurements provide better results in estimating the altitude of the quadcopter when compared to VIO, while in the x-axis provides slightly larger error (around .18 m), and it has comparable performance in the y-axis estimation. It should also be noted that the UWB technology with fixed anchors in the infrastructure provides a cm accuracy. Thus the obtained results cannot improve the UWB measurements for better accuracy due to technology limitations. However, the obtained results indicate the usage of UWB technology in multi-robot applications, while the aerial platform will be equipped with lower cost and lightweight sensors. Furthermore, Table 5 second column the RMSE values of the ground platform position, compared to Vicon are presented. As shown in Fig. 9, where the error is lower for the UWB-IMU data, it can be identified in the RMSE values as well. Finally, Table 5 third column the overall improved performance of the UWB-IMU estimates are reflected in the RMSE values for the relative positioning of the platforms.

5.2.2. Case 2: The ground platform navigates around the stationary quadcopter

For the second case, the quadcopter remains immobilized on top of an elevated flat surface while the quadruped robot starts to navigate. Similar to the previous scenario, the pilot performs maneuvers while changing the position and orientation of the ground platform around the quadcopter. Fig. 11 illustrates the position error estimates of the

Table 5
Case 1 — RMSE values between Vicon measurements and position estimated from VIO, UWB, and UWB fused with IMU for the quadcopter, ground platform, and the quadcopter position w.r.t ground platform.

	Quadcopter			Quadruped			Quadcopter w.r.t Quadruped		
	x	y	z	x	y	z	x	y	z
VIO	0.18	0.14	0.549	–	–	–	–	–	–
UWB	0.369	0.179	0.207	0.339	0.225	0.114	0.615	0.338	0.254
UWB-IMU	0.333	0.217	0.269	0.243	0.147	0.06	0.543	0.295	0.269

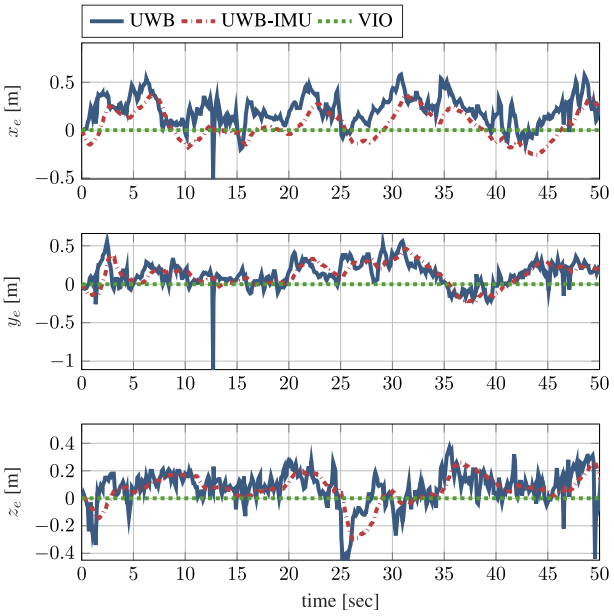

Fig. 11. Case 2 — Estimated global position error of immobilized the quadcopter with the proposed method with and without fused IMU data versus VIO.

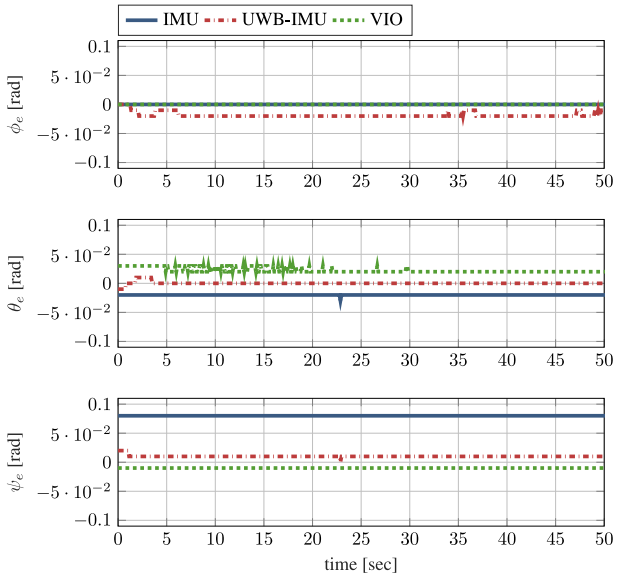

Fig. 12. Case 2 — Rotation error of the quadcopter w.r.t the ground platform.

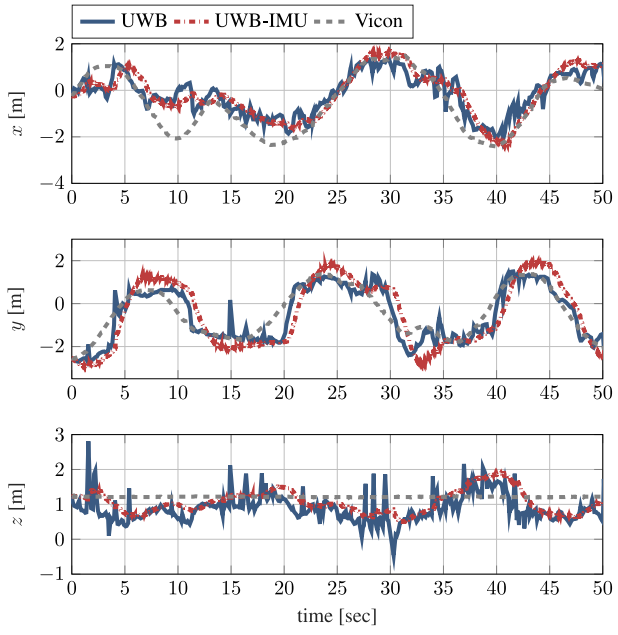

Fig. 13. Case 2 — Estimated global position of the ground platform of the proposed method with and without fused IMU data compared to Vicon measurements.

quadcopter in the global frame of the UWB measurements, UWB-IMU measurements, VIO. Since the aerial platform is not moving, the VIO measurements remain constant. It can be observed that UWB and UWB-IMU data fluctuate but remain under an error of 0.5 m except for some aggressive peaks.

Furthermore, it can be noticed that UWB-IMU appears to be smoother and fluctuates less when compared to UWB in all three axes. The ranges resulting from the UWB technology are subject to biases and unexpected stochastic variations. The result of those variations results in the fluctuation in position estimation from the optimization in (8). However, the IMU measurements are not indicating any changes. Thus the fusion of the UWB and IMU measurements increases the accuracy and omits these changes.

The rotation error of the stationary quadcopter, relative to the ground platform, remains constant and close to zero values, as depicted in Fig. 12. It is observed that the RMSE of the orientation measurements for all the measurements is very small since the platform is stationary and there is no excitation of the sensors. The combined orientation RMSE values are 0.011, 0.009, and 0.008 rad for the VIO, IMU, UWB-IMU, respectively.

For the same case, Fig. 13 presents the position of the ground platform based on UWB, UWB-IMU and Vicon data. The estimates of the x-axis for the initial 15 s deviate from the real values. While for the rest of the experiment, the estimates converge closer to the expected values. The estimates on the y-axis follow the Vicon data closely, while throughout the whole dataset, fluctuations of approximately 0.5 m appear in the altitude of the ground platform that, as indicated from the Vicon measurement and the nature of this experimental trial, it should be at a constant value.

Fig. 14 shows the position error of the ground platform between Vicon and UWB, UWB-IMU. The UWB-IMU presents larger error compared to the UWB for the y-axis in contrary to the other two axes. Overall the error is larger in the begging of the response.

Fig. 15 illustrates the quadcopter's and the ground platform's relative position error between Vicon measurements and UWB or UWB-IMU

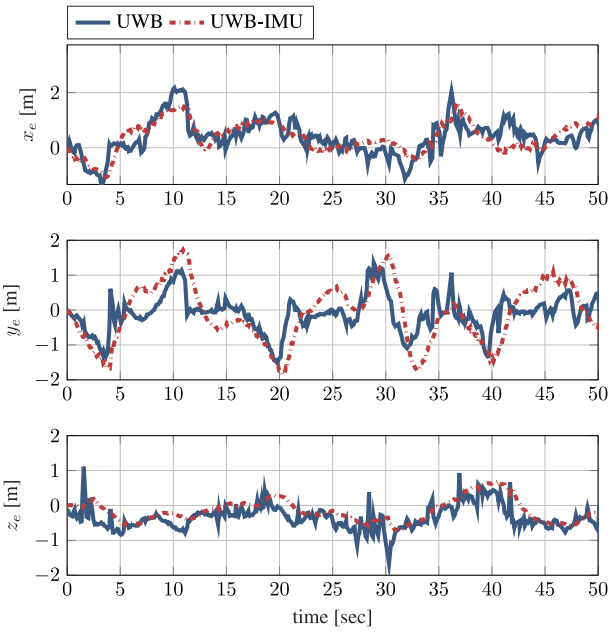

Fig. 14. Case 2 — Estimated global position error of the ground platform of the proposed method with and without fused IMU data.

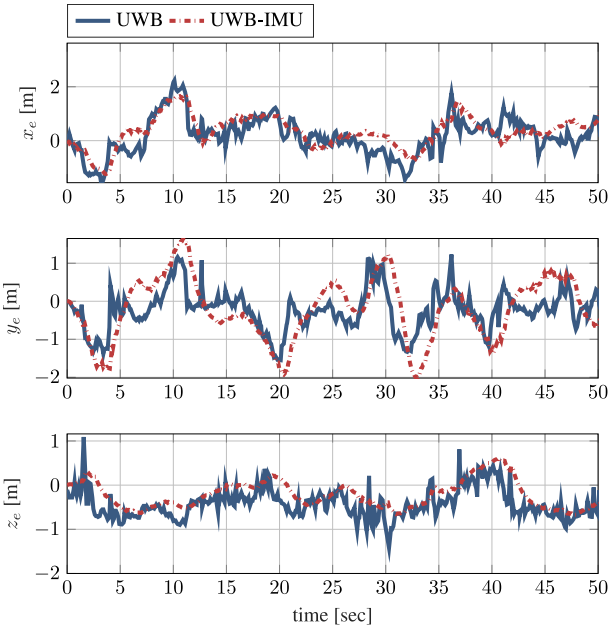

Fig. 15. Case 2 — Estimated relative position error of the quadcopter w.r.t the ground platform of the proposed method with and without fused IMU data.

estimates. Due to the higher uncertainty in the estimation of the ground platform, the relative position diverges slightly more than the Vicon data. Overall, the fused with IMU data appears to be smoother from UWB in terms of variations. In addition, it can be noticed that for this experimental trial, the x-axis appears to have a larger drift, while the y-axis of the UWB has a smaller error, and the z-axis error is bounded within 1 m.

Table 6 presents the RMSE values between the Vicon measurements and the VIO, UWB, UWB-IMU for the quadcopter and ground platform. The VIO has almost zero RMSE values while the platform remains stationary in the first column. On the other hand, considering that the

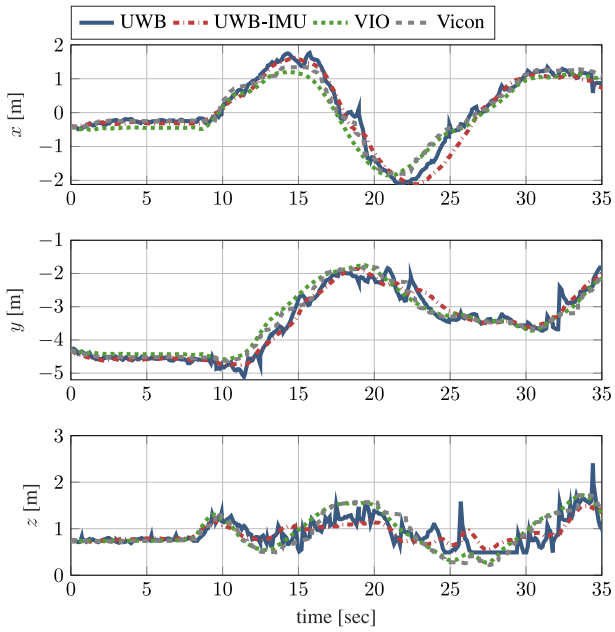

Fig. 16. Case 3 — Estimated global position of the quadcopter with the proposed method with and without fused IMU data versus VIO and Vicon measurements.

quadruped robot is moving, thus the reference UWB anchors are moving, the RMSE values for the position estimates are higher, as expected due to the vibrations and other uncertainties. It is also observed that the localization obtained from the UWB-IMU measurements provides better results in estimating the position of the quadcopter when compared to UWB in terms of RMSE. Table 6 in the second column shows the RMSE values between the Vicon measurements and the ground platform position obtained from the UWB and UWB-IMU measurements. Contrary to the previous case, where the ground platform was stationary, the vibrations due to the platform's motion create higher uncertainty on the ranges, which is reflected in the RMSE of position data. The UWB-IMU estimates have lower RMSE values on the x and z-axes. While on the y-axis, the UWB appears to be close to the Vicon measurements with lower RMSE. Finally, as presented in the last column of Table 6, the overall performance of the UWB-IMU and UWB estimates RMSE values are similar except the x-axis. The reason behind the lower performance of the x-axis can be linked with the installation of the UWB on the quadcopter, as they are fewer units and closer to each other, a series of outlier ranges that drop the estimation performance or false initial guess based on a false estimate.

5.2.3. Case 3: Simultaneous navigation of both platforms

The last experimental trial evaluates the performance of the proposed method during simultaneous navigation of both the aerial and ground platforms. Initially, the quadcopter is docked on the ground platform, and after a quick 90° rotation lets the aerial platform take-off and navigate. Immediately after the aerial platform reaches a safe distance, the quadruped starts to navigate in the same area. Fig. 16 illustrates the position estimates of the quadcopter in global frame of the UWB measurements, UWB-IMU, VIO, and Vicon measurements. For this experimental trial, it can be noticed that the position estimates are close to the Vicon data.

Fig. 17 shows the error between the Vicon measurements and the estimated UWB, UWB-IMU, and VIO positions of the quadcopter. The error remains almost zero in the first 10 s as the platform moves docked on the ground platform. Most of the time, the localization of the platform has an error under 0.5 m. Worth noting that in the x-axis the UWB-IMU has a drift that results in an error of 1 meter.

Table 6
Case 2 — RMSE values between Vicon measurements and position estimated from VIO, UWB, and UWB fused with IMU for the quadcopter, ground platform, and the quadcopter position w.r.t ground platform.

	Quadcopter			Quadruped			Quadcopter w.r.t Quadruped		
	x	y	z	x	y	z	x	y	z
VIO	0.003	0.003	0.002	–	–	–	–	–	–
UWB	0.257	0.208	0.151	0.719	0.513	0.472	0.694	0.619	0.527
UWB-IMU	0.166	0.194	0.126	0.666	0.647	0.362	0.681	0.710	0.382

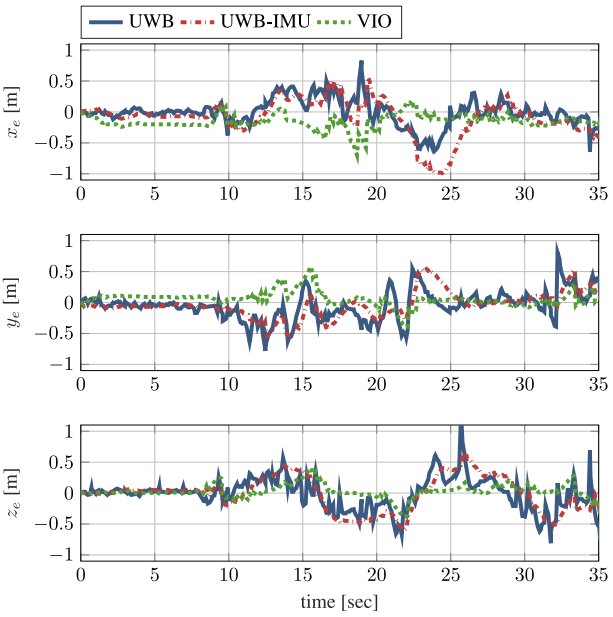

Fig. 17. Case 3 — Estimated global position error of the quadcopter between Vicon and the proposed method with and without fused IMU, and VIO.

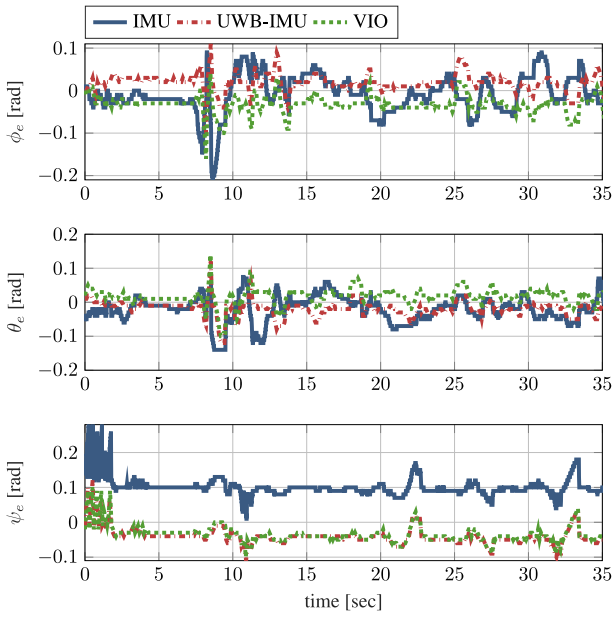

Fig. 18. Case 3 — Rotation error of the quadcopter w.r.t the ground platform0.

The rotation error of the quadcopter w.r.t the ground platform is presented in Fig. 18. Overall, the orientation data's accuracy is very similar to the Vicon measurements; however, it is noticeable a constant bias between the IMU and the UWB-IMU, VIO on the yaw of the platform. Furthermore, it is observed that the RMSE of the orientation is similar. The combined orientation RMSE values are 0.037, 0.035, and 0.034 rad for the VIO, IMU, UWB-IMU, respectively.

Fig. 19 shows the estimated global position error between the "true" values of the ground platform and the UWB, UWB-IMU. In this case, it is likely to expect a lower positioning performance when both platforms are navigating simultaneously due to the small distance among the UWB transceivers (Table 3) on the aerial platform side, vibrations of both platforms during motion, and outliers due to the communication of the UWB transceivers. By eliminating these factors and increasing the distance between the UWB units on the aerial platform, better performance can be expected.

Finally, Fig. 20 illustrates the relative position error data between the UWB, the UWB-IMU and Vicon data. It is observed that the estimation of the position on y is more accurate when compared to the x and z axes.

The performance of the third scenario is reflected in the respective RMSE information in Table 7. The quadcopter has the least RMSE values. The VIO appears to have the least error but only approximately 0.1 m less than the UWB estimated positions error. In addition, although in Fig. 16 the UWB-IMU data appear to be smoother than UWB. Furthermore, the ground platform's RMSE values appear to be higher compared to the quadcopter. The UWB appear to have smaller error values compared to the UWB-IMU. This difference in RMSE values between the UWB and the UWB-IMU data is a result of the initial performance of the UWB position estimation. The last column of

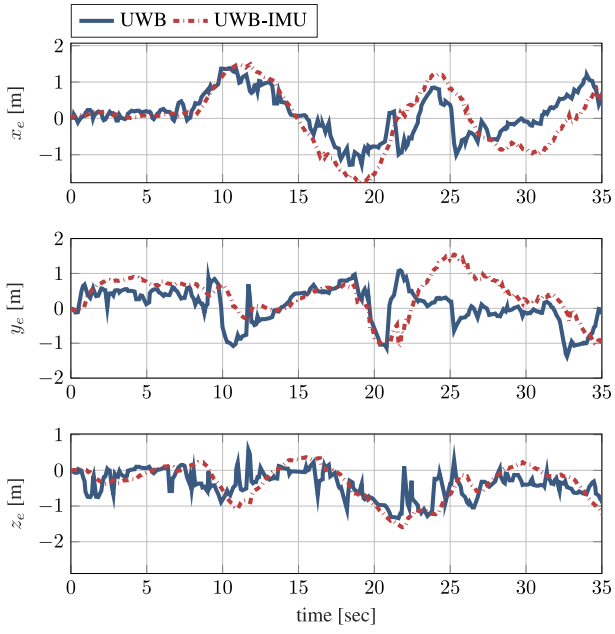

Fig. 19. Case 3 — Estimated global position error of the ground platform of the proposed method with and without fused IMU data.

Table 7 presents the RMSE of the relative position. It can be noticed that the overall error is very similar between the UWB and the UWB-IMU data for the y and z axes, while for the x-axis, the error is higher of

Table 7
Case 3 — RMSE values between Vicon measurements and position estimated from VIO, UWB, and UWB fused with IMU for the quadcopter, ground platform, and the quadcopter position w.r.t ground platform.

	Quadcopter			Quadruped			Quadcopter w.r.t Quadruped		
	x	y	z	x	y	z	x	y	z
VIO	0.190	0.133	0.122	–	–	–	–	–	–
UWB	0.218	0.240	0.262	0.609	0.526	0.539	0.662	0.674	0.539
UWB-IMU	0.233	0.229	0.289	0.818	0.669	0.6	0.942	0.698	0.558

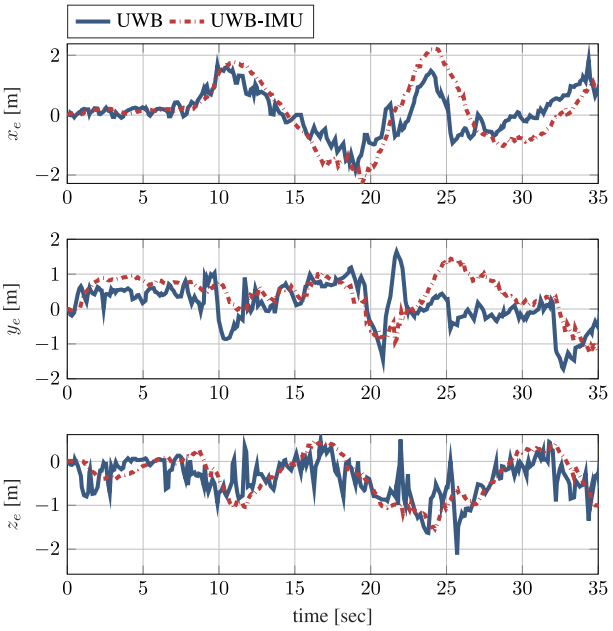

Fig. 20. Case 3 — Estimated relative position error of the quadcopter w.r.t the ground platform of the proposed method with and without fused IMU.

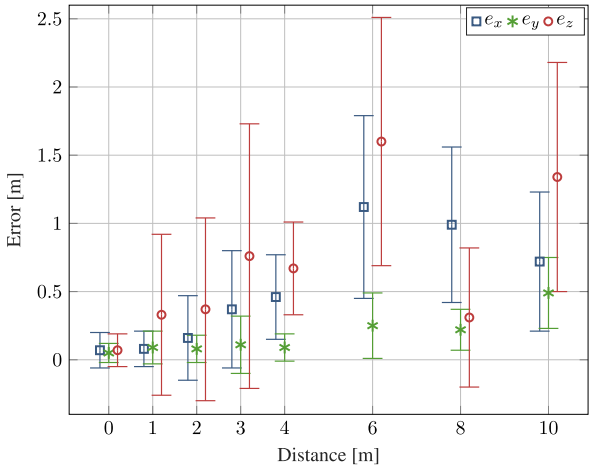

Fig. 21. Estimated and actual relative position error for different distances between the platforms.

UWB-IMU. RMSE of the relative position is affected mainly by the estimated values of the ground platform.

6. Discussion on performance

Several theoretical and technical observations have been made worth pointing out throughout the experimentation. This section discusses in detail the selection of the UWB placement and the effect of the extended UWB modules in the estimated values—an additional experimental shows the performance of the estimation as the distance between the platforms increases—a discussion on the advantages of switching to adaptive weights.

6.1. Placement of UWB and vibrations

As presented during the initial testing, we observed "jumps" on the z-axis measurements due to the close installation of the UWB nodes. A fifth elevated UWB is installed to reduce the amount of "jumps" and improve the z-axis accuracy. The UWB's extended installation creates a swinging effect during the motion of the robot that can affect the ranging information. However, it has been found through experimentation to provide significant consistency on the measurements instead of affecting the accuracy of the pose. Installing the module closer to the body can significantly reduce the swinging effect at the cost of a few extra "jumps" on the z-axis. Additionally, software filtering of the distance measurements can be implemented to reduce the noise caused by vibrations in all UWB modules. Furthermore, a hardware-oriented solution would be using dampeners or gimbals in conjunction with the extender (if there is one) to improve accuracy further while maintaining the measurements' consistency.

6.2. Effect of UWB's modules placement

The platforms placed immobilized at eight different distances in between them. More specifically, when the aerial platform is docked on the ground platform and at approximately 1, 2, 3, 4, 6, 8, and 10 meters apart (limited by the size of the room hosting the Vicon system). Then we ran the estimation for 40 s, and we measured the deviation of each axis from the actual distance after the optimization converges. Fig. 21 compares the distance between the two platform versus the estimated positions error. The $e_{x,y,z}$ denotes the RMSE between the actual value (Vicon measurement) and the estimated relative position of the quadcopter w.r.t the ground platform. The RMSE values shown with square, star, circle markers for x, y, z axes respectively denote the estimated positions' accuracy while the error's variance, shown as error bars, denotes the precision of the estimates.

While the distance between the platforms increases, the estimated relative position accuracy, and precision decrease. That indicates an upper limit on the in-between distance of two platforms, after which the accuracy of the estimates decays. Furthermore, we can notice that the y-axis estimates are both more precise and accurate regardless of the distance between the robots. Additionally, the least accurate estimates are on the z-axis, as identified during all the experiments. These findings indicate an open research question for the optimal placement of the UWB transceivers to improve the estimates when the nodes have to be installed close to each other.

6.3. Adaptive parameters

Throughout the experimentation in this study, the tuning parameters for the optimization were kept constant for comparison purposes. It would be challenging to maintain the same parameters if the platforms were operating in a more dynamic environment than the lab's controlled conditions. The proposed framework has several parameters that can be adjusted online to improve performance in certain conditions. Nowadays, robotic systems include complex sensor suites, which can

be advantageous for providing an accurate *initial guess* in contrary to relying on the previously estimated value. Additionally, the weight $\boldsymbol{Q}_0$ can be updated based on the variances of the system, indicating the level of trust we have in the past states. Finally, the measurement window N can be increased or decreased based on the availability of computation resources, thus increasing the window when the demand is low and vice versa when the computation demands are already high.

7. Conclusion and future work

This work established a theoretical framework for the estimation of the relative pose between two robots based on UWB ranges and IMU rotations without the need of fixed infrastructure. As it has been shown through extensive experiments for three different cases, the individual robots could successfully estimate the global and relative pose of the other robot. Nevertheless, the performance it is highly linked with the accuracy of the respective ranges, which are used for the optimization. Thus, it has been shown that as closer to each other the transceivers are installed, the estimation performance reduces correspondingly. In the experimental validation, it has been identified that in all the three presented cases it was more difficult to estimate the position of the quadruped when the transceivers acting as "anchors" were installed on the quadcopter were very close to each other. In addition, it has been shown when the position data is fused with orientation data based on IMU, the estimates seems to be more accurate. Yet, the UWB-IMU data can be characterized to be smoother, while some data spikes are successfully filtered out.

Future work will focus on the technical aspect to improve the optimization stage with initialization components, fusion with onboard sensors for improved pose estimation, numerical efficiency. In addition, the method's performance can be evaluated outside of a laboratory in a harsher environment with more sensors, which can further address the limitations and challenges. The current theoretical framework can be expanded further to estimate the 3D body rotation. While the platform's initial relative pose is still a prerequisite, the problem will be decoupled from the use of IMU, thus without requiring continuous communication between robots when it is not required. Finally, the utilization of the relative pose estimation will be investigated further in various robotic applications with a primary focus on multi-agent systems.

CRediT authorship contribution statement

Andreas Papadimitriou: Conceptualization, Methodology, Software, Validation, Investigation, Writing – original draft, Writing – review & editing. **Sina Sharif Mansouri:** Conceptualization, Methodology, Validation, Investigation, Writing – original draft, Supervision. **George Nikolakopoulos:** Resources, Supervision, Writing – review & editing, Project administration.

Declaration of competing interest

The authors declare that they have no known competing financial interests or personal relationships that could have appeared to influence the work reported in this paper.

References

Agha, A., Otsu, K., Morrell, B., Fan, D. D., Thakker, R., Santamaria-Navarro, A., et al. (2021). NeBula: Quest for robotic autonomy in challenging environments TEAM CoSTAR at the DARPA subterranean challenge.

Alapetite, A., Wang, Z., Hansen, J. P., Zajaczkowski, M., & Patalan, M. (2020). Comparison of three off-the-shelf visual odometry systems. *Robotics*, *9*(3).

Bouman, A., Ginting, M. F., Alatur, N., Palieri, M., Fan, D. D., Touma, T., et al. (2020). Autonomous spot: Long-range autonomous exploration of extreme environments with legged locomotion. In *2020 IEEE/RSJ international conference on intelligent robots and systems* (pp. 2518–2525). IEEE.

Eleftheroglou, N., Mansouri, S. S., Loutas, T., Karvelis, P., Georgoulas, G., Nikolakopoulos, G., et al. (2019). Intelligent data-driven prognostic methodologies for the real-time remaining useful life until the end-of-discharge estimation of the lithium-polymer batteries of unmanned aerial vehicles with uncertainty quantification. *Applied Energy*, *254*, Article 113677.

Fresk, E., Ödmark, K., & Nikolakopoulos, G. (2017). Ultra wideband enabled inertial odometry for generic localization. *IFAC-PapersOnLine*, *50*(1), 11465–11472.

Funabiki, N., Morrell, B., Nash, J., & Agha-mohammadi, A.-a. (2020). Range-aided pose-graph-based SLAM: Applications of deployable ranging beacons for unknown environment exploration. *IEEE Robotics and Automation Letters*, *6*(1), 48–55.

Güler, S., Abdelkader, M., & Shamma, J. S. (2019). Infrastructure-free multi-robot localization with ultrawideband sensors. In *2019 American control conference* (pp. 13–18).

Guo, K., Li, X., & Xie, L. (2020). Ultra-wideband and odometry-based cooperative relative localization with application to multi-UAV formation control. *IEEE Transactions on Cybernetics*, *50*(6), 2590–2603.

Jeong, Y., & Kweon, I. S. (2013). Relative pose estimation for an integrated UGV-UAV robot system. In J. Lee, M. C. Lee, H. Liu, & J. -H. Ryu (Eds.), *Intelligent robotics and applications* (pp. 625–636). Berlin, Heidelberg: Springer Berlin Heidelberg.

Kanellakis, C., Fresk, E., Mansouri, S. S., Kominiak, D., & Nikolakopoulos, G. (2020). Towards visual inspection of wind turbines: A case of visual data acquisition using autonomous aerial robots. *IEEE Access*, *8*, 181650–181661.

Kanellakis, C., Mansouri, S. S., Georgoulas, G., & Nikolakopoulos, G. (2018). Towards autonomous surveying of underground mine using MAVs. In *International conference on robotics in Alpe-Adria Danube region* (pp. 173–180). Springer.

Kanellakis, C., Mansouri, S. S., & Nikolakopoulos, G. (2017). Dynamic visual sensing based on MPC controlled UAVs. In *2017 25th Mediterranean conference on control and automation* (pp. 1201–1206). IEEE.

Kelsey, J. M., Byrne, J., Cosgrove, M., Seereeram, S., & Mehra, R. K. (2006). Vision-based relative pose estimation for autonomous rendezvous and docking. In *2006 IEEE aerospace conference* (pp. 20–pp). IEEE.

Mansouri, S. S., Kanellakis, C., Fresk, E., Kominiak, D., & Nikolakopoulos, G. (2018). Cooperative coverage path planning for visual inspection. *Control Engineering Practice*, *74*, 118–131.

Mansouri, S. S., Kanellakis, C., Kominiak, D., & Nikolakopoulos, G. (2020). Deploying MAVs for autonomous navigation in dark underground mine environments. *Robotics and Autonomous Systems*, Article 103472.

Mueller, M. W., Hamer, M., & D'Andrea, R. (2015). Fusing ultra-wideband range measurements with accelerometers and rate gyroscopes for quadrocopter state estimation. In *2015 IEEE international conference on robotics and automation* (pp. 1730–1736).

Nguyen, T. -M., Hanif Zaini, A., Wang, C., Guo, K., & Xie, L. (2018). Robust target-relative localization with ultra-wideband ranging and communication. In *2018 IEEE international conference on robotics and automation* (pp. 2312–2319).

Özaslan, T., Loianno, G., Keller, J., Taylor, C. J., Kumar, V., Wozencraft, J. M., et al. (2017). Autonomous navigation and mapping for inspection of penstocks and tunnels with MAVs. *IEEE Robotics and Automation Letters*, *2*(3), 1740–1747.

Pizarro, O., Eustice, R., & Singh, H. (2003). Relative Pose Estimation for Instrumented, Calibrated Imaging Platforms. In *Proc. seventh digital imaging computing, techniques and applications conf* (pp. 601–612).

na Queralta, J. P., Qingqing, L., Schiano, F., & Westerlund, T. (2020). VIO-UWB-based collaborative localization and dense scene reconstruction within heterogeneous multi-robot systems.

Reif, K., Gunther, S., Yaz, E., & Unbehauen, R. (1999). Stochastic stability of the discrete-time extended Kalman filter. *IEEE Transactions on Automatic Control*, *44*(4), 714–728.

Shule, W., Almansa, C. M., na Queralta, J. P., Zou, Z., & Westerlund, T. (2020). UWB-based localization for multi-UAV systems and collaborative heterogeneous multi-robot systems. *Procedia Computer Science*, *175*, 357–364.

Solà, J. (2017). Quaternion kinematics for the error-state Kalman filter.

Song, H., Choi, W., & Kim, H. (2016). Robust vision-based relative-localization approach using an RGB-depth camera and LiDAR sensor fusion. *IEEE Transactions on Industrial Electronics*, *63*(6), 3725–3736.

Yaakov, B. -S., X., R. L., & Thiagalingam, K. (2004). State estimation for nonlinear dynamic systems, chapter 10. In *Estimation with applications to tracking and navigation* (pp. 371–420). John Wiley & Sons, Ltd.